Journal of Molecular Liquids 390 (2023) 123046

Contents lists available at ScienceDirect

Journal of Molecular Liquids

journal homepage: www.elsevier.com/locate/molliq

Effect of percolation on the deformation of isotropic electrorheological elastomers under external electric fields

Barnabás Horváth [a,*], Sándor Guba [a], Diána Balogh [b], Miklós Jakab [c], István Szalai [a,b]

[a] Research Centre for Engineering Sciences, Mechatronics and Measurement Techniques Research Group, University of Pannonia, 10 Egyetem St, H-8200 Veszprém, Hungary

[b] Institute of Mechatronics Engineering and Research, University of Pannonia, 18/A Gasparich Márk St, H-8900 Zalaegerszeg, Hungary

[c] Research Centre for Engineering Sciences, Department of Materials Engineering, University of Pannonia, 10 Egyetem St, H-8200 Veszprém, Hungary

ARTICLE INFO

Keywords:
Electrorheological elastomers
Field-induced deformation
Percolation
Electrical conductivity
Dielectric permittivity

ABSTRACT

In this study we investigate the influence of the filler's concentration with an emphasis on the percolation of particles on the field-induced deformation of isotropic, disc shaped electrorheological elastomers (EREs) with barium titanate filler. It was found that above the percolation threshold concentration (>34.7 wt%) the magnitude of the fully reversible contraction was enhanced by a factor of ~10 in the low field strength region ($E \approx 0.2$ MVm^{-1}). At higher field strength ($E = 1.1$ MVm^{-1}) the percolation had no effect on the induced strain, and regardless of the particle's concentration it saturated around 1.2%. It was shown that for isotropic EREs the optimal particle loading is just above the percolation threshold. If the filler content exceeds the threshold concentration, then the same deformation can be achieved with much lower field intensity, but even larger particle concentration does not enhance the performance further.

1. Introduction

Smart materials, which respond to changes of their environment play a prominent role among modern multifunctional materials. Numerous of these materials are composites, where solid inclusions are embedded in a cross-linked polymer matrix. Depending on the magnetic or dielectric properties of the solid particles a macroscopic response (e.g. rheological, mechanical, etc.) can be stimulated either by external magnetic or electric fields (or in special cases by the combination of the two). The macroscopic response arises largely from the coupling between the dipole-dipole interactions of the embedded particles (which carry (magnetic or electric) dipole moments induced by the external field) [1] and the particle-matrix interactions. The latter determines the mobility of the solid phase, therefore the response depends to a large extent on the elasticity of the polymer matrix. For example, ferrogels display a pronounced mechanical response, due to the low elasticity of the loosely cross-linked, dilute polymer network [2,3]. As it was shown by experimental studies ferrogel bodies could undergo a relatively large deformation (on the order of 40% or even larger) when exposed to magnetic fields [4]. On the other hand, the magnetic particles in magnetorheological elastomers (MREs) are bonded to a matrix with high degree of polymerization, which has a relatively large elastic modulus, therefore their field-induced mechanical response is reduced (on the order of a few %).

Likewise, the electric counterparts of MREs – the electrorheological elastomers (EREs) – are usually composed of micro- or nanometer-sized dielectric particles embedded in an elastic polymer matrix (silicone rubber, polyurethane, etc.) with a larger elastic modulus (1 MPa - 20 MPa) [5]. The magnitude of the electric field-induced dipole moment of the particles – which primarily affects the macroscopic response – is proportional to the dielectric permittivity difference between the particles and the matrix. For that reason, usually materials with large dielectric permittivity are chosen for the filler, such as ferroelectric materials (e.g. barium titanate [6–8]), or highly polarizable conjugated polymers [9,10].

Besides the change in rheological properties, the dipole-dipole interactions between the polarized particles cause a macroscopic deformation, thus the dimensions of an ERE body can be also manipulated with an external electric field [11]. A reversible deformation is achievable in a controllable manner, therefore EREs have found various technological applications where the field-induced deformation and/or the variable elastic modulus is exploited in the field of actuators [12,13], vibration

* Corresponding author.
E-mail addresses: horvath.barnabas@mk.uni-pannon.hu (B. Horváth), guba.sandor@mk.uni-pannon.hu (S. Guba), balogh.diana@mk.uni-pannon.hu (D. Balogh), jakab.miklos@mk.uni-pannon.hu (M. Jakab), szalai.istvan@mk.uni-pannon.hu (I. Szalai).

https://doi.org/10.1016/j.molliq.2023.123046
Received 14 May 2023; Received in revised form 31 August 2023; Accepted 9 September 2023
Available online 17 September 2023

control [14,15], tunable metamaterials [16], etc. Because of technical and economic reasons high performing EREs are required for such applications, which can achieve the desired deformation at lower operating field strength and with lower particle loading [17].

The performance of EREs from the viewpoint of practical applications depends primarily on the micro- and mesostructure [18], and the shape of the ERE body. The shape contribution to the overall deformation stemming from the geometry (i.e. aspect ratio) is positive along the external field. On the other hand, the structural contribution depends strongly on the short range arrangement of the particles in the matrix, which is affected by the concentration, shape, and size distribution of the solid phase, thus it can be either positive or negative and varies highly in its magnitude. The relative contribution of these two effects determines the magnitude of the overall deformation, and whether the elastomer body contracts or expands in the direction of the uniform field [19,20]. In general, the performance can be enhanced with an anisotropic microstructure [21], when the particles are pre-aligned in chain like clusters with an electric field during the fabrication process. However, in case of isotropic EREs with random particle distribution the nature of the microstructure changes abruptly with increasing filler content when the percolation threshold is reached [22]. If the concentration of the filler is below the percolation threshold, then the particles are isolated and relatively far away from each other. Above the percolation threshold the microstructure transitions into a connected network spanning the whole volume of the ERE body. Because the percolated structure acts as a conductive pathway, the electrical conductivity and dielectric properties of the elastomers also change drastically with the microstructure [23].

In the present work, the main focus is on how the formation of a percolated particle network affects the macroscopic deformation (i.e. electrostriction) of isotropic EREs. For this purpose we have synthesized barium titanate filled model EREs, and investigated the dependence of the electric field-induced deformation on the concentration of the filler particles. Furthermore, the relationship between the particle content and the electrical conductivity, and dielectric properties is also investigated, with an emphasis on the percolation.

2. Experimental

2.1. Preparation of EREs

Disc shaped, isotropic ERE bodies with different concentration of barium titanate ($BaTiO_3$) filler were fabricated. The $BaTiO_3$ powder (American Elements) had an average particle diameter of < 1.5 μm, tetragonal crystal structure, and it was used as supplied. The elastomer matrix was Elastosil RT604 A/B addition-curing, two component silicone rubber (polydimethylsiloxane, PDMS) by Wacker. Component A contained the platinum catalyst, while the crosslinker was in component B. The $BaTiO_3$ filler was dispersed in component A and after that component B was added. The solid loading of the prepared EREs was varied between 10% and 55% by weight. The exact compositions together with the volumetric concentrations are listed in Table 1. The range of the particle loading of our samples is similar to concentration of EREs used in typical applications, but this varies highly with the chemical composition of the particles. The ratio of the silicone rubber components A and B was 9 to 1 by weight in all cases. Triton X-100 nonionic surfactant was used in a concentration of 1% by weight to aid the dispersion of the particles in the liquid components. The mixture was homogenized by vigorous stirring for 30 minutes, and the air bubbles were removed under vacuum for 25 minutes. The liquid mixture was poured into the mold, and the polymerization process was carried out at $T = 120\,^{\circ}C$ in a drying oven. The samples achieved final strength after 40 minutes. The size of the cylindrical ERE discs was $d = 19$ mm in diameter with a height of $h_0 = 5.5$ mm (height-to-width aspect ratio of 1:3.5). Fig. 1 shows examples of the ERE discs.

Table 1
Composition of the fabricated elastomer samples.

Sample	$BaTiO_3$ content	
	c (wt%)	v (vol%)
0B-ERE	–	–
10B-ERE	10.0	1.8
20B-ERE	20.0	3.9
30B-ERE	30.0	6.5
35B-ERE	35.0	8.0
40B-ERE	40.0	9.7
50B-ERE	50.0	13.9
55B-ERE	55.0	16.5

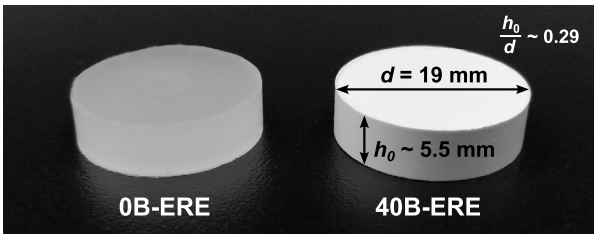

Fig. 1. Dimensions of the fabricated ERE discs with different barium titanate loading (the left disc is the PDMS elastomer without filler particles).

2.2. Measurement methods

2.2.1. Electric field-induced deformation

To measure the deformation of the EREs along the direction of an external electric field an optical contour method was applied [24]. The schematic diagram of the measurement setup is shown in Fig. 2. The elastomer body was placed on an electrically grounded stainless steel platform, which served as a ground electrode. The electrode on the top surface of the ERE was made of thin aluminum foil (top electrode), which had the same diameter as the ERE sample. Both surfaces of the elastomer were painted with conductive silver varnish for better electrical contact between the elastomer and the electrodes.

The external electric field was created between the top and the ground electrode by connecting the positive terminal of a high voltage power supply (HCP 14-12500, FuG Elektronik GmbH) to the top electrode. The electric field was parallel with the axis of the cylindrical ERE bodies. The voltage across the electrodes was varied between 0 and 6000 V, thus the maximum of the external electric field strength was $E = 1.1\ \mathrm{MVm^{-1}}$. It should be noted, that inside the elastomer body the electric field strength is different from the externally applied field due to the induced polarization. The distribution and strength of the internal field depends on the shape and the ϵ dielectric permittivity of the material. For the disc shaped EREs with low aspect ratio the internal field can be approximated as $E_i \approx E/\epsilon$ [26]. The maximum of E was chosen to remain below the limit imposed by the dielectric strength of the elastomers. The range of the field strength covers the lower range of typical values used in real applications [25], however in some cases even stronger fields are used ($> 3\ \mathrm{MVm^{-1}}$). Due to the deformation of the elastomers in the direction of the field the electrode gap – and with that the field strength – also changes. However, the measured deformation was smaller than 1.3% in all cases, thus this change in the field strength was ignored.

On the top electrode a sharp-edged plastic target was placed, which could move freely with the top electrode, and follow the deformation of the elastomer body. The contour of the target's edge served as a reference line to detect the deformation in the axial direction. We note, that with this arrangement the deformation perpendicular to the direction of the field can not be observed. The ERE disc with the target on its top surface was illuminated from the back with an LED backlight to obtain a well defined contour. The position of the edge was monitored with a videomicroscope system made from a Point Grey Flea3 camera and

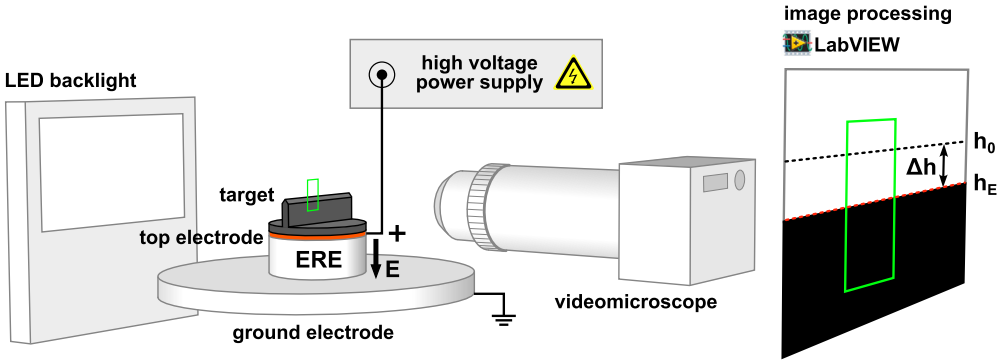

Fig. 2. Schematic diagram of the optical contour method for the measurement of the electric field-induced deformation.

a microscope objective lens (4×/0.12). The magnification of the camera system was chosen so that only a portion of the reference line was visible to detect the movement with high resolution (1.6 μm/pixel).

In a custom made LabVIEW program the video stream of the camera was processed in real-time, and on each frame the horizontal position of the reference line was determined with image processing algorithms. The average of twenty frames were used to calculate the position of the line at a given electric field strength. According the resolution of the camera system the relative change in position (compared to the original height h_0, when $E = 0$) was converted into relative change in height: $\Delta h = h_E - h_0$. Because the top electrode completely covered the top of the disc any inhomogeneous microdeformations of the surface were averaged by the target. Therefore, the measured deformation Δh was characteristic for the whole cross section. The strain as the ratio of the total deformation to the original dimension was also calculated: $\alpha = \Delta h / h_0$. The combined weight of the target and the upper electrode was so small that the compressive stress caused by it deformed the ERE discs only by a negligible amount (< 0.011%). No additional stress was applied to the ERE discs, therefore, the field-induced deformation was measured starting from a stress-free state. With our measurement method the deformation can be determined with an error smaller than 12%.

2.2.2. Electrical conductivity and dielectric properties

The complex dielectric permittivity $\hat{\epsilon}(\omega)$ of the ERE discs was measured by a capacitive parallel plate method at frequencies ranging from $f = 1$ kHz to $f = 1$ MHz. The ERE disc was placed between the electrodes of an Agilent 16451B dielectric test fixture as a dielectric to form a capacitor. The capacitance C_p and electrical resistance R_p of the fixture was measured with an Agilent 4284A impedance analyzer according a parallel RC model. The real and imaginary parts of $\hat{\epsilon}(\omega) = \epsilon'(\omega) - i\epsilon''(\omega)$ (where $\omega = 2\pi f$ is the angular frequency, and i is the imaginary unit) was calculated as

$$\epsilon' = \frac{h_0 C_p}{\epsilon_0 A_e}, \tag{1}$$

and

$$\epsilon'' = \frac{h_0}{2\pi f R_p \epsilon_0 A_e}, \tag{2}$$

where h_0 is the height of the ERE disc, which is equal to the electrode gap, A_e is the cross section of the guarded electrode and ϵ_0 is the vacuum permittivity. From Eq. (2) the ac conductivity can be also expressed as:

$$\sigma_{ac} = \frac{h_0}{R_p A_e} = \epsilon'' \epsilon_0 2\pi f . \tag{3}$$

The dc electrical conductivity of the ERE discs was measured with an IM6 megohmmeter (RE Technology). The sample was sandwiched between two stainless steel electrodes. The test voltage was $U = 100$ V. From the measured electrical resistance of the fixture (R) the dc conductivity of the ERE sample was calculated according the equation

$$\sigma_{dc} = \frac{h_0}{RA}, \tag{4}$$

where A is the cross section of the sample. All dielectric measurements were conducted at a temperature of $T = 21\,°C$.

2.2.3. Morphology of the particle structure

To observe the particle structure of the elastomer samples with different particle loading cross sectional images were taken with a scanning electron microscope (SEM). An Apreo SEM (Thermo Fisher) was used at an acceleration voltage of 20.0 kV.

3. Results and discussion

3.1. Percolation threshold

The dielectric spectra (the real and imaginary parts of the complex permittivity as a function of the frequency) of the EREs with different particle loading are shown in Fig. 3. The elastomers have shown no dielectric relaxation in the tested frequency range. Above 35 wt% filler content ϵ' increased towards low frequencies, which can be attributed to the Maxwell-Wagner polarization. This is typical for inhomogeneous elastomers, and it is caused by the interfacial polarization at the dielectric boundary layer between the solid particles and the elastomer matrix. In the lower frequency region ϵ'' also increased (especially above 35 wt%) approximately with a slope of -1 (on a log-log scale), which confirms a dc type electrical conduction. ϵ' and ϵ'' are extracted from the dielectric spectra at selected frequencies and their dependence on the concentration of the filler together with the ac and dc electrical conductivity is presented in Figs. 4(a), 4(b), and 4(c). The ac conductivity was calculated according to Eq. (3).

The dc conductivity of the elastomers increases abruptly by orders of magnitude when the particle concentration is larger than 35 wt% (Fig. 4(c)). The sharp change in the conductivity indicates the percolation of the $BaTiO_3$ particles, because the connected particle network, which spans the whole volume of the ERE disc, acts as electrically conductive pathways. We used the classical percolation theory [27] to model the dc conductivity of the EREs above the threshold concentration c_c:

$$\sigma_{dc} = \sigma_0 (c - c_c)^t , \tag{5}$$

where σ_0 is a constant depending on the conductivity of the filler, and t is the critical exponent. The exact percolation threshold c_c was determined according the linearized form of Eq. (5) and varying c_c until a best linear fit was achieved. The $\log \sigma_{dc}$ vs. $\log(c - c_c)$ plot is shown in Fig. 4(d) together with the best linear fit. The percolation threshold was $c_c = (34.7 \pm 0.1)$ wt% (7.9 vol%), while the critical exponent was $t = 1.45$.

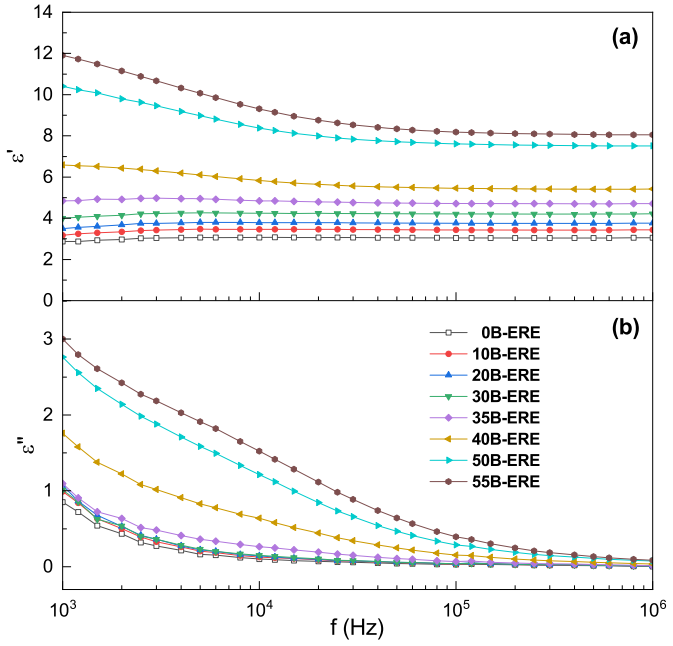

Fig. 3. The frequency dependent real (a) and imaginary (b) part of the complex permittivity at different filler concentrations.

The percolation threshold determined from the dc conductivity correlates well with the threshold concentration where the ac conductivity (and thus ϵ'') of the elastomers begins to increase rapidly at low frequencies ($f \sim 1$ kHz) (Figs. 4(b) and 4(c)). We note however, that at higher frequencies ($f \geq 10$ kHz) the data indicates that the sharp increase starts at lower concentration (around $c \sim 30$ wt%), but to verify such a shift of the limit with the frequency better accuracy and higher resolution of the concentration around the percolation threshold would be needed. Below the limiting concentration the ac conductivity and ϵ'' is basically independent from the particle loading, which is in line with that the larger distance between the particles would hinder the formation of conductive pathways.

The addition of $BaTiO_3$ particles causes an increase of the real part of the permittivity even below the percolation limit, but only by a small amount: from the $\epsilon' = 3.04$ permittivity of the pure PDMS matrix up to $\epsilon' = 4.71$. The permittivity is independent from the frequency until $c < c_c$. Beyond the percolation threshold a larger, frequency dependent increment is observed and the permittivity of the 55B-ERE reaches 11.91 at $f = 1$ kHz (see Fig. 4(a)). If we compare our dielectric data to other available results for similar $BaTiO_3$/PDMS EREs a very good agreement can be seen. For example, the results of Namitha et al. [28] show an $\epsilon' \approx 7.8$ (at 1 MHz) for a $BaTiO_3$ content of ~16 vol%, while the corresponding value of our 55B-ERE sample is $\epsilon' = 8.05$.

The SEM images presented in Fig. 5 confirm that there are directly detectable changes in the particle structure around the percolation threshold. At $c = 10$ wt% the majority of the randomly dispersed particles are isolated, and only a few particle clusters (due to incomplete homogenization) are visible. As the concentration is increased the number of clusters is also increasing, and at $c = 35$ wt% longer strands of touching particle clusters are also present. At $c = 40$ wt% most of the particles are part of the clusters and strands, and only a few isolated particle can be seen. We note, that the complete 3D particle network can not be seen in the SEM images, since these show only the 2D cross section of the ERE bodies, but the observed clusters and strands can be interpreted as the parts of the randomly branched three-dimensional network, which are close to the surface.

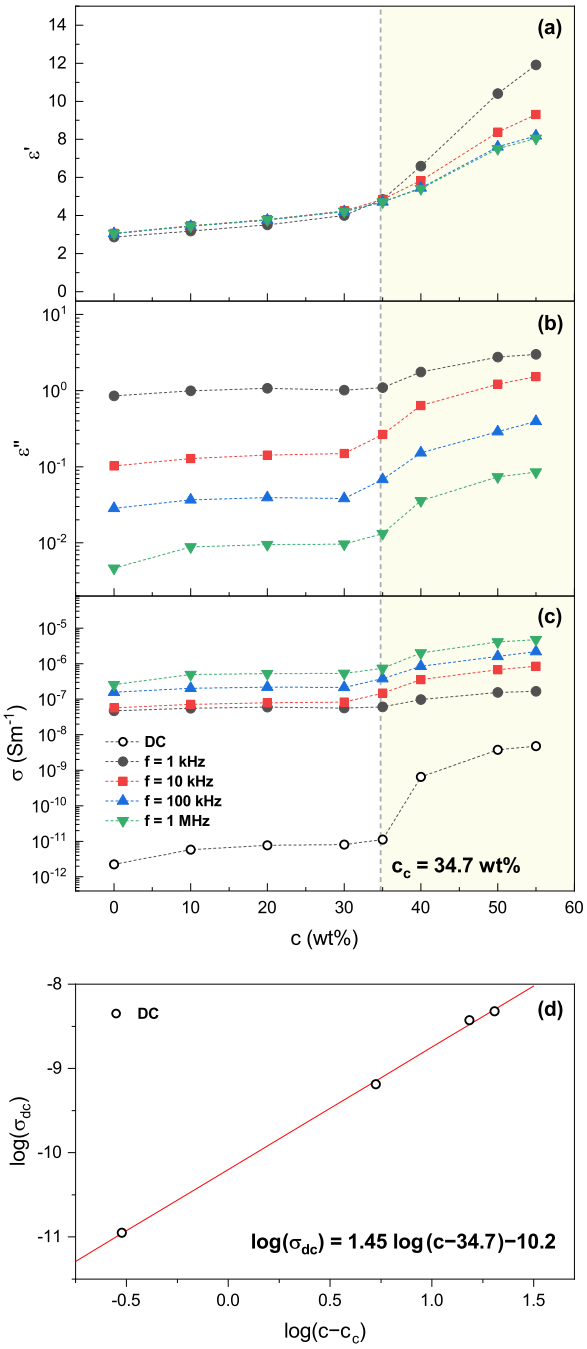

Fig. 4. The frequency dependent real (a), and imaginary (b) part of the complex permittivity, the dc (hollow symbols) and ac electrical conductivity (c) as the function of the $BaTiO_3$ content. The best linear fit (solid red line) of the $\log(\sigma_{dc})$ vs. $\log(c - c_c)$ plot (d) gives the percolation threshold ($c_c = 34.7$ wt%), which is marked by the vertical dashed lines on subfigures (a), (b), and (c).

3.2. Concentration dependence of the field-induced deformation

The strain (α) as a function of the external electric field strength in case of EREs with different particle loading is shown in Fig. 6. The electric field applied to the EREs was increased step-wise, starting from zero, and gradually approaching $E = 1.1$ MVm^{-1}. At each step it was held constant for 10 seconds before the corresponding strain was determined. The deformation was fully reversible, the ERE discs regained their original height after the electric field was removed.

All samples contracted ($\alpha < 0$) in the direction of the field. Contraction of field sensitive elastomer bodies is the result of the coupling be-

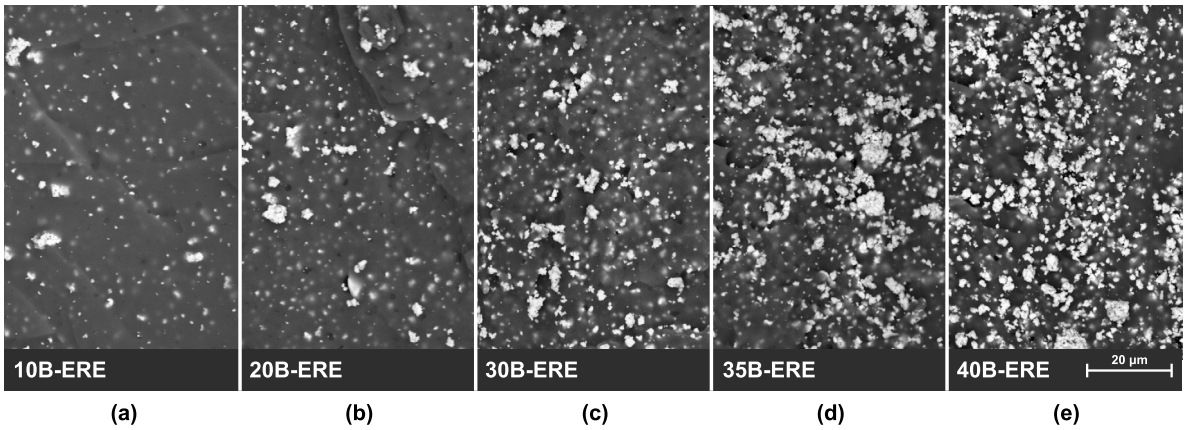

Fig. 5. Cross sectional SEM images of the EREs with increasing particle loading (form 10 wt% (a) to 40 wt% (e)).

tween the electrostriction of the elastomer body itself and the Maxwell effect. The latter is caused by the attractive Coulomb force between the oppositely charged electrodes, which exerts compressive stress on the elastomer body. In case of EREs the electrostriction is dominant, and the contribution of the Maxwell effect to the total contraction is usually less than 5% [29,30]. The magnitude of the strain due to the Maxwell effect can be calculated as $S_M = -(\epsilon_0 \epsilon' E^2)/(2Y)$, where Y is the Young's modulus of the elastomer [30], which was determined by force-strain measurement. The largest Maxwell effect would be shown by the 55B-ERE sample (largest ϵ') at the maximum electric field strength. In this case the estimated magnitude of the Maxwell effect was 0.33% of the total measured field-induced strain. All other samples would show smaller Maxwell effect, therefore it is considered that in our case α is purely the result of the electrostriction of the material.

The electrostriction of EREs is usually explained by the basic microscopic model of dipole-dipole interaction between particles carrying induced dipole moments, which is coupled with particle-elastic matrix interaction. As it was mentioned earlier (see Introduction) the overall deformation is the sum of this structural effect and the always positive contribution of the macroscopic shape effect. However, at small aspect ratios like in the case of our samples ($\sim$ 0.29) the macroscopic shape effect is weak, and the structural contribution is dominant. The latter can have either a positive or negative sign with varying magnitude as it was shown by simulation results [20]. For example, isotropic EREs contract along the field in most cases, but if the particle structure is approximated by body- or face-centered cubic structure, then elongation (i.e. positive electrostriction) is expected. To further highlight the complexity of the behavior of these systems and the importance of the microstructure we note, that according to our previous results [24] for the analogous magnetic case, the isotropic MRE bodies (with randomly dispersed iron particles in PDMS matrix) elongated in the direction of the magnetic field. This is in contrast with the behavior of isotropic EREs used here despite the same elastic matrix and similar macroscopic size and shape. Again, the cause of this difference could lie in the dissimilarity of the microstructure due to the difference in particle shape and size distribution.

As Fig. 6 shows, the magnitude of the contraction increased with E, although two regions can be distinguished in regard of the field strength. Under weak fields $|\alpha|$ grows fast with the external field strength. The trend is quadratic in this region, as it is shown by the fitted curves (in the form of $\alpha = kE^2$, where k is a fitting parameter) in Fig. 6. This corresponds to the theoretical models and general observation, that the electrostriction scales with the square of the electric field strength [31]. However, in stronger fields $|\alpha|$ approaches a saturation value, and increasing E further does not cause larger contraction. Similar nonlinear behavior, when the quadratic trend turns into saturation is often observed in case of other types of composite elastomers too [30]. The maximum of α was between $\alpha = -0.0107$ and

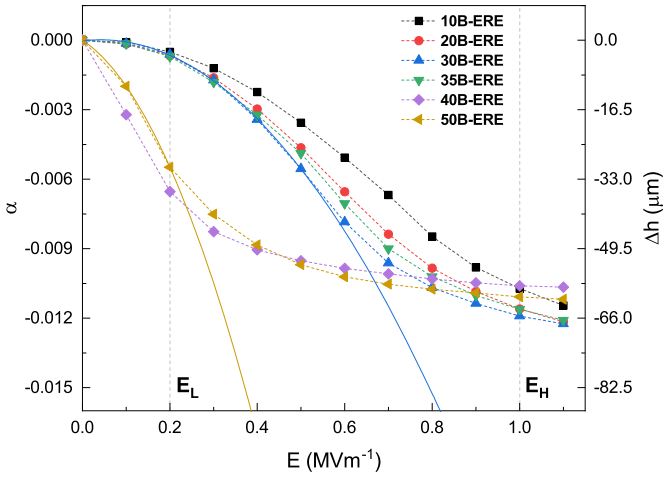

Fig. 6. The deformation response of the EREs with different particle loading (symbols) to electric fields. The trend with increasing field strength (dashed lines) changes significantly if the particle loading exceeds the percolation threshold (samples 40B-ERE and 50B-ERE). The solid lines show the quadratic fit in the low field strength region in case of 30B-ERE and 50B-ERE.

$\alpha = -0.0122$, which corresponds to a characteristic absolute deformation of $\Delta h = (-59 \pm 3)$ μm and $\Delta h = (-67 \pm 8)$ μm, respectively. In case of EREs, where the field-induced deformation is pure electrostriction (the Maxwell effect is negligible) these values are typical and are similar to other ERE materials [30].

The transition region of E, where the initial quadratic trend changes into the approach towards saturation depends greatly on the concentration of the filler. Up to c = 35 wt% particle loading the EREs behave similarly: the transition region of E is above 0.5 MVm^{-1}. In contrast, if the particle concentration is beyond the percolation threshold (40 wt% or larger), then the magnitude of α increases much faster with the field strength, and the transition into saturation occurs already above 0.2 MVm^{-1}.

The significant difference in the behavior of the EREs with different particle loading is further emphasized in Fig. 7, where α is shown as the function of the filler's concentration at low and high field strengths. In the lower field strength region ($E_L = 0.2$ MVm^{-1}) the magnitude of the contraction increases approximately tenfold if the concentration of the $BaTiO_3$ particles exceeds 35 wt%, which correlates very well with the percolation threshold determined according the dc conductivity. Since with the onset of the percolation the local arrangement of the particles is significantly altered compared to a random distribution (e.g. the interparticle distance is reduced) it is not surprising that it influences the deformation to a large extent. The structural effect stemming from the

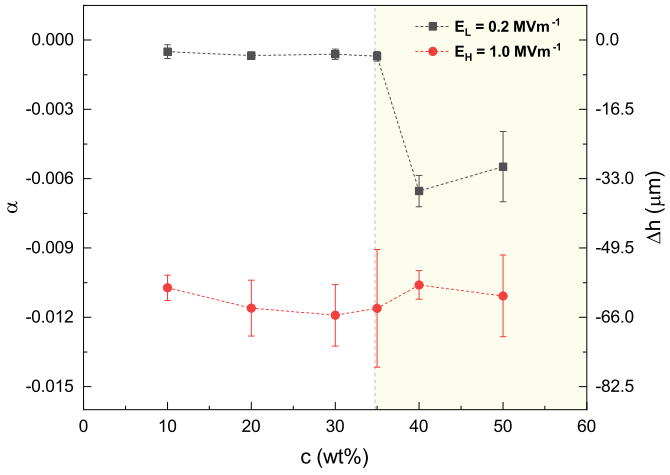

Fig. 7. Concentration dependence of the field-induced deformation at different field strengths. The concentration where the abrupt change in the magnitude of the deformation occurs (at lower field strengths (E_L)) corresponds to the percolation threshold (marked by the vertical dashed line). In stronger fields (E_H) the deformation is independent from the filler's concentration.

dipole-dipole interactions becomes stronger as the interparticle distance is reduced, thus the response to electric field is greatly enhanced if the particles are close to each other in a connected network. On the other hand, increasing the particle loading beyond the percolation limit does not increase the magnitude of the deformation significantly, because the particle structure becomes so dense that the local rearrangement of the particles is hindered by each other. This can be seen in Figs. 6 and 7 as the EREs with 40 wt% and 50 wt% filler concentration show nearly the same response. Moreover, at higher field strength ($E_H = 1.0$ MVm^{-1}), when the saturation of the deformation occurs, α becomes independent of the concentration, and all EREs have similar maximal deformation ($|\alpha| \sim 0.012$).

4. Conclusions

Disc shaped (1:3.5 aspect ratio), PDMS-based electrorheological elastomers with different $BaTiO_3$ filler content were synthesized, and their deformation under axial electric fields was studied. The following main results were obtained.

- The synthesized ERE bodies contracted along the direction of the field – parallel with their axis – and regained their original height when the field was switched off. The magnitude of the contraction changed quadratically with E in the low field strength region, which transitioned into saturation at higher field strengths.
- The field-induced deformation response was affected largely by the presence of a percolated particle structure. The percolation threshold of the $BaTiO_3$ particles according the dc electrical conductivity was $c_c = (34.7 \pm 0.1)$ wt% (7.9 vol%), where the dielectric permittivity also changed significantly. The change of the particle structure around the percolation threshold was directly confirmed by SEM images.
- Above the percolation threshold the magnitude of the field-induced contraction is enhanced by a factor of ~10 in the low field strength region ($E \approx 0.2$ MVm^{-1}). At high field strength the percolation has no effect on the magnitude of the contraction. All samples regardless of the particle concentration had almost the same maximum reduction in height, which was on the order of ~ 65 μm (~ 1.2% of the original height) at $E = 1.1$ MVm^{-1}.

The results show that if lower operating field strength is required to maximize the performance of EREs, then the filler content should exceed the percolation threshold, because the same deformation can be achieved with much lower field intensity. On the other hand, even larger particle concentration does not enhance the performance further, thus the optimal particle loading is just above the percolation threshold.

As it was pointed out, the notable effect of the microstructural changes due to the percolation on the deformation could be explained qualitatively mainly by the distance dependent nature of the dipole-dipole interactions. However, it is evident that taking into account only the interactions between the dipoles hindered by an elastic matrix does not offer a complete description of the relationship between the particle structure and the field-induced deformation. Thus, to capture every aspect of the complex behavior of these materials, and to find answers to open questions further experimental and theoretical works are required.

CRediT authorship contribution statement

Barnabás Horváth: Conceptualization, Formal analysis, Investigation, Methodology, Software, Validation, Visualization, Writing – original draft, Writing – review & editing. **Sándor Guba:** Conceptualization, Formal analysis, Investigation, Methodology, Validation, Writing – original draft, Writing – review & editing. **Diána Balogh:** Conceptualization, Formal analysis, Investigation, Methodology, Validation, Writing – original draft. **Miklós Jakab:** Investigation. **István Szalai:** Conceptualization, Formal analysis, Funding acquisition, Methodology, Project administration, Resources, Supervision, Validation.

Declaration of competing interest

The authors declare that they have no known competing financial interests or personal relationships that could have appeared to influence the work reported in this paper.

Data availability

All data generated and analyzed during this study are available from the corresponding author on reasonable request.

Acknowledgements

This work was supported by the TKP2020-NKA-10 project financed under the 2020-4.1.1-TKP2020 Thematic Excellence Programme by the National Research, Development and Innovation Fund of Hungary. We are also gratefully acknowledging the financial support of the National Research, Development, and Innovation Office – NKFIH K137720.

References

[1] P. Metsch, H. Schmidt, D. Sindersberger, K.A. Kalina, J. Brummund, G.K. Auernhammer, G.J. Monkman, M. Kästner, Field-induced interactions in magneto-active elastomers - A comparison of experiments and simulations, Smart Mater. Struct. 29 (2020) 085026, https://doi.org/10.1088/1361-665X/ab92dc.

[2] A. Safronov, E. Mikhnevich, Z. Lotfollahi, F. Blyakhman, T. Sklyar, A. Larrañaga Varga, A. Medvedev, S. Fernández Armas, G. Kurlyandskaya, Polyacrylamide ferrogels with magnetite or strontium hexaferrite: next step in the development of soft biomimetic matter for biosensor applications, Sensors 18 (2018) 257, https://doi.org/10.3390/s18010257.

[3] D.S. Wood, P.J. Camp, Modeling the properties of ferrogels in uniform magnetic fields, Phys. Rev. E 83 (2011) 011402, https://doi.org/10.1103/PhysRevE.83.011402.

[4] A.P. Safronov, A.Yu. Zubarev, E.A. Mikhnevich, E.V. Rusinova, A kinetic model for magnetostriction of a ferrogel with physical networking, Philos. Trans. R. Soc. A 379 (2021) 20200315, https://doi.org/10.1098/rsta.2020.0315.

[5] X. Dong, C. Niu, M. Qi, Electrorheological elastomers, IntechOpen (2017), https://doi.org/10.5772/intechopen.68396.

[6] W. Liu, Z. Xie, Y. Lu, M. Gao, W. Zhang, L. Gao, Fabrication and excellent electroresponsive properties of ideal PMMA@BaTiO 3 composite particles, RSC Adv. 9 (2019) 12404–12414, https://doi.org/10.1039/C9RA01174A.

[7] A. Kumar, D. Ahmad, K. Patra, Barium titanate particle filled silicone elastomer composite: preparation and evaluation of morphology and mechanical behaviour, J. Phys. Conf. Ser. 1240 (2019) 012049, https://doi.org/10.1088/1742-6596/1240/1/012049.

[8] L. Gao, L. Zhan, W. Liu, Y. Zhang, Z. Xie, J. Ren, Preparation and electro responsive properties of Mg-doped BaTiO3 with novel morphologies, J. Mater. Sci., Mater. Electron. 30 (2019) 12107–12112, https://doi.org/10.1007/s10854-019-01568-7.
[9] R. Kunanuruksapong, A. Sirivat, Poly(p-phenylene) and acrylic elastomer blends for electroactive application, Mater. Sci. Eng. A 454–455 (2007) 453–460, https://doi.org/10.1016/j.msea.2006.12.033.
[10] K. Thongsak, R. Kunanuruksapong, A. Sirivat, W. Lerdwijitjarud, Electroactive polydiphenylamine/poly(styrene-block-isoprene-block-styrene) (SIS) blends: effects of particle concentration and electric field, Mater. Sci. Eng. C 31 (2011) 206–214, https://doi.org/10.1016/j.msec.2010.08.022.
[11] J. Fehér, G. Filipcsei, J. Szalma, M. Zrínyi, Bending deformation of neutral polymer gels induced by electric fields, Colloids Surf. A, Physicochem. Eng. Asp. 183–185 (2001) 505–515, https://doi.org/10.1016/S0927-7757(01)00562-3.
[12] X. Yuan, X. Zhou, Y. Liang, L. Wang, R. Chen, M. Zhang, H. Pu, S. Xuan, J. Wu, W. Wen, A stable high-performance isotropic electrorheological elastomer towards controllable and reversible circular motion, Composites, Part B, Eng. 193 (2020) 107988, https://doi.org/10.1016/j.compositesb.2020.107988.
[13] A.M. Bazinenkov, D.A. Ivanova, A.P. Rotar', V.P. Mikhailov, Actuator based on a dielectric elastomer with quartz as a filler for vacuum technology, IOP Conf. Ser., Mater. Sci. Eng. 781 (2020) 012007, https://doi.org/10.1088/1757-899X/781/1/012007.
[14] N. Ma, Y. Yao, Q. Wang, C. Niu, X. Dong, Properties and mechanical model of a stiffness tunable viscoelastic damper based on electrorheological elastomers, Smart Mater. Struct. 29 (2020) 045041, https://doi.org/10.1088/1361-665X/ab7736.
[15] K. Wei, Q. Bai, G. Meng, L. Ye, Vibration characteristics of electrorheological elastomer sandwich beams, Smart Mater. Struct. 20 (2011) 055012, https://doi.org/10.1088/0964-1726/20/5/055012.
[16] Y. Xu, Y. Li, L. Cao, Z. Yang, X. Zhou, Steering of SH wave propagation in electrorheological elastomer with a structured meta-slab by tunable phase discontinuities, AIP Adv. 7 (2017) 095114, https://doi.org/10.1063/1.4996245.
[17] D.J. Levine, K.T. Turner, J.H. Pikul, Materials with electroprogrammable stiffness, Adv. Mater. 33 (2021) 2007952, https://doi.org/10.1002/adma.202007952.
[18] C. Cao, X. Zhao, Tunable stiffness of electrorheological elastomers by designing mesostructures, Appl. Phys. Lett. 103 (2013) 041901, https://doi.org/10.1063/1.4816287.
[19] O.V. Stolbov, Y.L. Raikher, Magnetostriction effect in soft magnetic elastomers, Arch. Appl. Mech. 89 (2019) 63–76, https://doi.org/10.1007/s00419-018-1452-0.
[20] E. Allahyarov, H. Löwen, L. Zhu, A simulation study of the electrostriction effects in dielectric elastomer composites containing polarizable inclusions with different spatial distributions, Phys. Chem. Chem. Phys. 17 (2015) 32479–32497, https://doi.org/10.1039/C5CP05522A.
[21] B.D. Chin, M.-S. Chun, H. Henning Winter, Modulus-switching viscoelasticity of electrorheological networks, Rheol. Acta 48 (2009) 177–189, https://doi.org/10.1007/s00397-008-0326-8.
[22] R.M. Mutiso, K.I. Winey, Electrical conductivity of polymer nanocomposites, in: Polymer Science: A Comprehensive Reference, Elsevier, 2012, pp. 327–344.
[23] C.O. Blattmann, S.E. Pratsinis, Nanoparticle filler content and shape in polymer nanocomposites, KONA 36 (2019) 3–32, https://doi.org/10.14356/kona.2019015.
[24] D. Balogh, S. Guba, B. Horváth, I. Szalai, Magnetic field-induced deformation of isotropic magnetorheological elastomers, Magnetochemistry 8 (2022) 146, https://doi.org/10.3390/magnetochemistry8110146.
[25] X. Zhou, L. Wang, D. Huang, Y. Liang, Q. Shi, H. Yaying, M. Zhang, H. Pu, W. Wen, J. Wu, Smart table tennis racket with tunable stiffness for diverse play styles and unconventional technique training, Adv. Mater. Technol. 6 (2021) 2100535, https://doi.org/10.1002/admt.202100535.
[26] Y. Shiau, A.R. Valentino, ELF electric field coupling to dielectric spheroidal models of biological objects, IEEE Trans. Biomed. Eng. BME-28 (1981) 429–437, https://doi.org/10.1109/TBME.1981.324815.
[27] M. Rahaman, A. Aldalbahi, P. Govindasami, N.P. Khanam, S. Bhandari, P. Feng, T. Altalhi, A new insight in determining the percolation threshold of electrical conductivity for extrinsically conducting polymer composites through different sigmoidal models, Polymers 9 (2017) 527, https://doi.org/10.3390/polym9100527.
[28] L.K. Namitha, M.T. Sebastian, High permittivity ceramics loaded silicone elastomer composites for flexible electronics applications, Ceram. Int. 43 (2017) 2994–3003, https://doi.org/10.1016/j.ceramint.2016.11.080.
[29] J. Su, J.S. Harrison, T.L.St. Clair, Y. Bar-Cohen, S. Leary, Electrostrictive grafr elastomers and applications, MRS Proc. 600 (1999) 131, https://doi.org/10.1557/PROC-600-131.
[30] V. Cârlescu, G. Prisăcaru, D. Olaru, Electromechanical response of silicone dielectric elastomers, IOP Conf. Ser., Mater. Sci. Eng. 147 (2016) 012057, https://doi.org/10.1088/1757-899X/147/1/012057.
[31] G. Diguet, J.-Y. Cavaille, G. Sebald, T. Takagi, H. Yabu, A. Suzuki, R. Miura, Physical behavior of electrostrictive polymers. Part 1: polarization forces, Comput. Mater. Sci. 190 (2021) 110294, https://doi.org/10.1016/j.commatsci.2021.110294.